SAMI: the SCAO module for the E-ELT adaptive optics imaging camera MICADO

Y. Clénet[a], P. Bernardi[a], F. Chapron[a], E. Gendron[a], G. Rousset[a], Z. Hubert[a], R. Davies[b], M. Thiel[b], N. Tromp[c] and R. Genzel[b]

[a]LESIA, UMR 8109 CNRS, Observatoire de Paris, Université Paris Diderot, 5 place Jules Janssen, 92190 Meudon, France;
[b] Max Planck Institute for extraterrestrial Physics, Postfach 1312, 85741 Garching, Germany
[c] NOVA-ASTRON, P.O.Box 2, Dwingeloo, Netherlands

ABSTRACT

SAMI, the SCAO module for the E-ELT adaptive optics imaging camera MICADO, could be used in the first years of operation of MICADO on the telescope, until MAORY is operational and coupled to MICADO. We present the results of the study made in the framework of the MICADO phase A to design and estimate the performance of this SCAO module

Keywords: E-ELT, MICADO, SCAO, adaptive optics, simulation, design

1. SAMI TOP-LEVEL REQUIREMENTS

MICADO (Davies et al., 2010), the Multi-AO Imaging Camera for Deep Observations, has being designed to work with adaptive optics (AO) on the E-ELT. The instrument is intended to image, through selected wide and narrow-band near infrared filters, a wide field of view (∼60") at the E-ELT diffraction limit. It is primarily intended to work with the multi conjugate AO (MCAO) system MAORY (Diolaiti et al., 2010). Though, MAORY is not expected to be fully operational and available for MICADO at the MICADO first light, hence the need for a simpler AO system, an internal single conjugate AO (SCAO) module, SAMI (ScAo module for MIcado), that will deliver on-axis diffraction-limited images allowing one to cover parts of the MICADO science cases.

The SCAO module being not part of the original ESO call for proposal, the SAMI top-level requirements (TLR) were established so that SAMI-MICADO interfaces remain as close as possible to MAORY-MICADO ones. The SAMI TLR were also established having in mind that the SCAO module will be used only during the first years of MICADO operations and could consequently work with restrained specifications (e.g., field of view). The SAMI top-level requirements were the following:

- patrol field of view: 45"

- wavefront sensor (WFS) bandpass: 0.45-0.8 μm

- repositioning accuracy: 2 mas for small dithers (i.e. $\pm$0.3 mas offsets within few tenths of second with AO loop closed) and for large dithers (i.e. few arcseconds offsets within up to 30 seconds with AO loop open during offset but closed at both positions)

- relay optics image quality: 80% at 0.8 μm

- relay optics magnification: 1

- SCAO module transmission: 80%

- SCAO module above MICADO in a gravity invariant position

One should note that we have been asked to study a visible wavefront sensor. Though, in conjunction with science case priorities, this choice could be revisited in a Phase B to study the implementation of an infrared wavefront sensor or both an infrared and a visible wavefront sensor.

Further author information: (Send correspondence to Y. Clénet)
Y. Clénet.: E-mail: yann.clenet at obspm.fr, Telephone: +33145077548

Adaptive Optics Systems II, edited by Brent L. Ellerbroek, Michael Hart, Norbert Hubin, Peter L. Wizinowich,
Proc. of SPIE Vol. 7736, 77363Q · © 2010 SPIE · CCC code: 0277-786X/10/$18 · doi: 10.1117/12.856602

2. SAMI OPTO-MECHANICAL DESIGN

SAMI will actually ensure four functionalities, each of them corresponding to a dedicated subsystem:

- provide an optical relay between the telescope beam and MICADO,
- derotate the field while the telescope tracks the scientific target,
- deliver to MICADO an AO corrected beam thanks to a dedicated WFS,
- support the MICADO cryostat on the E-ELT Nasmyth platform.

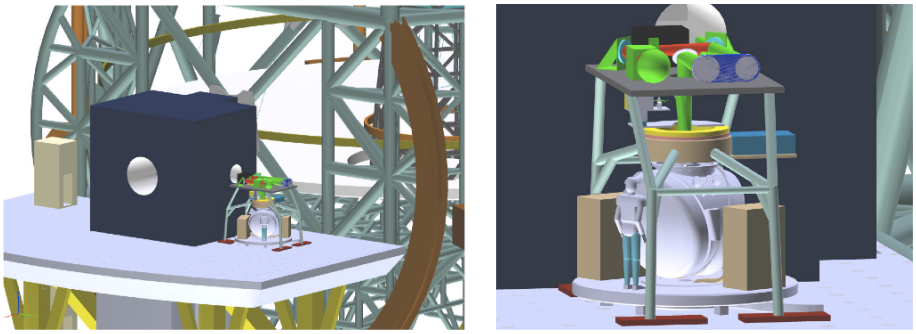

Figure 1. Global views of MICADO and SAMI mounted on the E-ELT Nasmyth platform

2.1 Weight and cost

Table 1. SAMI weight and cost

Item	Mounting structure	Derotator	Optical relay	WFS	Total
Mass (kg)	2000	610	1471	168.5	2610
Cost (k€)	68	36	96	374 (camera: 140)	574

2.2 The relay optics

Given the too small back focal distance of the E-ELT (750 mm), an optical relay has to be included into the beam between the E-ELT pre-focal station flange and the MICADO focal plane. This relay is made of: (i) a 3-mirror Offner relay (M7, M8 and M9), mounted and fixed on an optical bench, (ii) a folding mirror (M10) that directs the beam downward to the dichroic plate and MICADO, (iii) a dichroic plate, reflecting the light between 0.45 and 0.8 μm towards the WFS and transmitting the light between 0.8 and 2.32 μm towards MICADO. A magnification of 1, similar to MAORY's one, has been adopted, leading to a scale of 3.605 mm/arcsec.

Table 2. Relay optics performances

Parameters	Specification	Design value
Field of view	45"	45"
F/#	17.71	17.71
Scale	3.605 mm/arcsec	3.605 mm/arcsec
Field curvature	1.3 m from MAORY, 43.8m from E-ELT	∞
Image quality	Strehl ratio at 0.8 μm greater than 80%	Strehl ratio at 0.8 μm greater than 80%
Exit pupil location	∞ from MAORY, -43.3m from ELT,	+77m
Back focal distance	500 mm	667.2 mm
Transmitted wavelength range	0.8 - 2.32 μm	0.8 - 2.32 μm

2.3 The derotator and support structure

MICADO being located at the E-ELT Nasmyth platform, a field derotator has to be provided to MICADO to compensate for the telescope movements. We assume a specification of the derotator to be able to rotate of 360° in about 20 min. The dichroic plate, M11, the wavefront sensor and MICADO are rotating together with the derotator. This derotator is included in a support structure. This structure supports both MICADO and the WFS assembly.

2.4 The M11 pupil steering mirror

This mirror, located just after the dichroic plate, picks off the WFS beam light and sends it to the WFS. This mirror is used to ensure several functions:

- since M7 and M9 are spherical, the exit pupil of the relay optics is not at infinity, but at 77m, resulting in tilted images. This effect is corrected by tilting M11. The maximum tilt angle is given by the field size at 77m: 170 mm/77 mm = 0.126°. Hence to correct for the impact of the exit pupil location, M11 has to be tilted of a maximum angle of ±0.063°, in rather large timescales (minutes),

- one has to correct for the E-ELT pupil run out. We assume this run out to be 1% of its diameter (a run out value for the Coudé focus is given in the ESO document *E-ELT interfaces for scientific instruments* but not for the Nasmyth focus, hence we assumed the same value as for the Coudé focus), which translates into 1/1771 = 0.034°. This run out is assumed to be very slow, on minute timescales,

- one has to correct the WFS K-mirror misalignment effects when this K-mirror rotates. We assumed a maximum tilt angle of ±1°.

Hence, the maximum tilt angle must be ±1°. The accuracy of these tilt corrections must be about 1/1000 of the pupil size, i.e. 1/17710= 3.24e-3 degrees.

2.5 The wavefront sensor

2.5.1 Overview

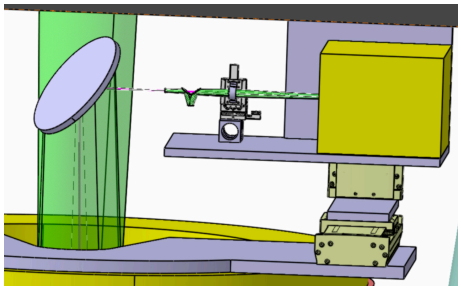

Figure 2. View of the WFS. On the left, the M11 mirror. On the right, the camera box, fixed on linear stages allowing the WFS to move in the field for reference star pick off and offsets/dithers. At the centre, the field stop, the K-mirror and the triplet.

SAMI's concept follows the recommandations of the ESO document *"Guidelines for the post-focal SCAO NGS wavrefront sensor for the E-ELT AO based instrumentation"*: the WFS is a Shack-Hartmann and we have adopted the recommended camera and detector characteristics. Hence, the camera dimensions are: width 340 mm × height 240 mm × depth 300 mm, and its weight is 10 kg. The detector readout noise is assumed to be 3 e^- and its quantum efficiency 85% inside the WFS bandpass (0.45-0.8 microns).

The WFS includes a field stop, a K-mirror, a lens triplet, the micro-lenses and the camera. To pick off the AO reference star, this whole assembly can move along X and Y directions in front of the M11 mirror. The total amplitude of these displacements, to cover the 45" field, is ±85 mm. The jitter specifications translate into a displacement of the WFS of ±1.08 mm (resp. 18 mm) in a fraction of second with a repositioning accuracy of 7 microns for small dithers (resp. large dithers).

The K-mirror function is to rotate the pupil of the WFS (see Section 2.5.2). We assume the mirrors to be mounted in a single assembly. The K-mirror will rotate at the same speed as the derotator, but in the opposite direction, hence a specification to be able to rotate of 360° in about 20 minutes.

2.5.2 Pupil and field rotation

In our baseline, we have chosen to have the WFS rotating together with M4, to ensure a proper conjugation of the microlenses with the M4 actuators. The alternative would have been to let the microlenses rotate with respect to M4 and to update in real time the AO control matrix. The latter solution has not been chosen since not considered as a mature technique and then too risky for MICADO regarding the will to adopt proven solutions.

Having the dichroic plate rotating also together with the WFS, we hence have the WFS, the dichroic plate and MICADO rotating together with the field. It implies to mount the WFS on a x/y stage for the reference source pick-off and the offsets/dithers and to include in the WFS a pupil rotation stage (the K-mirror). The alternative to this K-mirror would have been to rotate the whole WFS assembly together with the pupil but, once again, we have considered it as a too complex solution, given the possible rotation amplitudes.

2.5.3 ADC

The variation of the refraction index $n(\lambda)$ with respect to the wavelength induces a shift of the WFS spot with respect to the wavelength. This effect is modulated by the effective flux received from the reference source with respect to the wavelength, i.e. by the detector quantum efficiency and the reference source spectrum. It thus leads to an enlarged spot if no atmospheric dispersion corrector is inserted inside the WFS beam.

We consider the effective flux with respect to wavelength $\phi(\lambda)$ received on the detector as the product of the black body Planck law $PL(\lambda, T_{eff})$ of a M-type star (which represents about 90% of the stellar population) by the detector quantum efficiency $QE(\lambda)$ (whose characteristics are derived from the feasibility studies launched by ESO for large, fast low noise, visible detector for AO wavefront sensing ; J. Kolb, private communication) and the spectral window bandpass $W(\lambda, \lambda_{inf}, \lambda_{sup})$.

Considering $F(p)$ the flux received on the detector as a function of the position p on the detector, the flux conservation leads to:

$$F(p) = \frac{\phi(\lambda)}{dp/d\lambda} = \frac{PL(\lambda, T_{eff}) \times QE(\lambda) \times W(\lambda, \lambda_{inf}, \lambda_{sup})}{d\Delta R(\lambda, \lambda_0, z)/d\lambda} \tag{1}$$

where $\Delta R(\lambda, \lambda_0, z)$ is the atmospheric dispersion given in arcsec at the wavelength λ, the zenith distance z, with respect to the reference wavelength λ_0:

$$\Delta R(\lambda, \lambda_0, z) = 206264.8\,(n(\lambda) - n(\lambda_0))\tan z \tag{2}$$

The FWHM ΔG of the monochromatic spot function $G(p, \Delta G)$ has been computed with an home-made simulation tool of an AO loop for a single Shack-Hartmann subaperture (see Sect. 4.7.1 and Fig. 3). The polychromatic spot flux $f(p)$ is then given by the convolution of $F(p)$ with $G(p, \Delta G)$:

$$f = FFT^{-1}\left(FFT(F) \times \overline{FFT(G)}\right) \tag{3}$$

We can then evaluate the FWHM Δf of the polychromatic spot flux function $f(p)$ as a function of the shortest cut-off wavelength of the WFS bandpass. Hence, for typical M stars of the main sequence, the atmospheric dispersion enlarges the WFS spot up to ∼0.3" for the design atmospheric conditions at a zenith angle of 30° (Fig. 3).

In the photon noise regime, the WFS noise σ^2 is proportional to $\theta_b^2/np(\lambda_{inf}, \lambda_{sup})$ where θ_b is the size of the blurred WFS spot and $np(\lambda_{inf}, \lambda_{sup})$ is the number of photons per subaperture and per frame within the (λ_{inf},λ_{sup}) band-pass. Hence, the noise, $\sigma_0(z, 0.45)$ when using an ADC, at a given zenith angle z and for the entire WFS bandpass [0.45 μm, 0.8 μm] is given by:

$$\sigma_0^2(z, 0.45) = f^2(z, 0.45)/np_{w/\,ADC}(0.45) \tag{4}$$

Taking into account a WFS spot elongation by the atmospheric dispersion along only one direction and then separating the WFS noise into different x and y components, the noise when not using any ADC, at a given zenith angle z and for a WFS bandpass [λ_{inf},0.8 μm] is given by:

$$\sigma^2_{w/o\,ADC}(z, \lambda_{min}) = 0.5 \times \left(f^2(z, \lambda_{min}) + \Delta G^2(z, \lambda_{min})\right) / np_{w/o\,ADC}(\lambda_{min}) \tag{5}$$

The latter expression can be converted into an equivalent noise with an ADC $\sigma_{0\,eq}(z, 0.45)$ using a reducing factor α, which then represents a normalized equivalent number of photons:

$$\sigma^2_{0\,eq}(z, 0.45) = f^2(z, 0.45)/\alpha/np_{w/\,ADC}(0.45) \tag{6}$$

With a ADC transmission $t_{ADC}(\lambda)$=0.8, the number of photons without and with ADC ratio is equal to:

$$\frac{np_{w/o\,ADC}(\lambda_{min})}{np_{w/\,ADC}(0.45)} = \frac{\int_{\lambda_{inf}}^{0.8} PL(\lambda, T_{eff}) \times QE(\lambda) d\lambda}{\int_{0.45}^{0.8} PL(\lambda, T_{eff}) \times QE(\lambda) \times t_{ADC}(\lambda) d\lambda}, \tag{7}$$

the magnitude loss is then

$$-2.5 \log \left(\frac{2 \times f^2(z, 0.45)}{f^2(z, 0.45) + \Delta G^2(z, 0.45)} \frac{np_{w/o\,ADC}(\lambda_{min})}{np_{w/\,ADC}(0.45)} \right) \tag{8}$$

Hence, for typical M stars of the main sequence, the lack of ADC induces a magnitude loss of ∼0.1 mag (in the photon noise regime) for the design atmospheric conditions at a zenith angle of 30° (Fig. 3). A similar calculation can be made in the detector noise regime where the WFS noise is proportional to $\theta_b^4/np^2(\lambda_{inf}, \lambda_{sup})$. For typical M stars of the main sequence, the lack of ADC induces also a small magnitude loss in the detector noise regime for the atmospheric design conditions at a zenith angle of 30°.

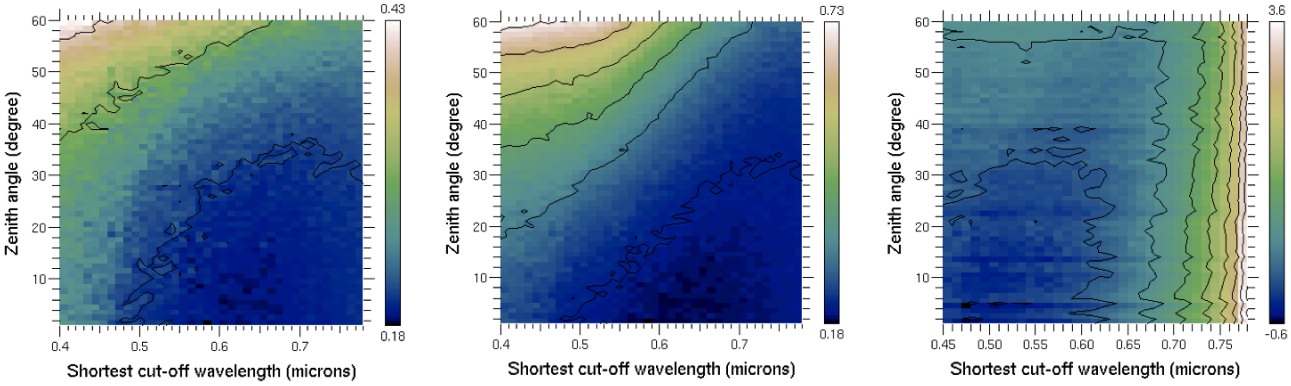

Figure 3. Left: WFS monochromatic spot FWHM ΔG, in arcsec. Contours are for 0.2", 0.3", 0.4". Centre: WFS polychromatic spot FWHM Δf, in arcsec, when no ADC is used and for T_{eff}=3300 K, as a function of the shortest WFS cut-off wavelength and of the zenith angle. Contours are for 0.2", 0.3", 0.4", 0.5", 0.6", 0.7". Right: Magnitude loss when no ADC is used in photon noise regime, for T_{eff}=3300 K, with respect to the case with an ADC and a WFS bandpass of [0.45 μm - 0.8 μm], as a function of the shortest WFS cut-off wavelength and of the zenith angle. Contours are for a magnitude loss from -0.5 to 3.5 equally spaced by 0.5

3. THERMAL BACKGROUND ANALYSIS

This analysis is done with the following assumptions:

- atmospheric transmission: T_{atm}=95%,

- K-band zero point from the "ESO database of technical data for E-ELT simulations" (www.eso.org/sci/facilities/eelt/science/drm/tech_data/): F_0=4.37×10^9 photons/s/m^2/μm

- K-band sky brightness (ESO document "E-ELT AO design inputs: relevant atmospheric parameters"): m_{sky}=13 arcsec^{-2}

- telescope transmission T_{tel}: five mirrors with protected silver/aluminium coatings (transmission profile from the "ESO database of technical data for E-ELT simulations"),

- telescope area A_{tel}=1276.82 m^2 ("ESO database of technical data for E-ELT simulations"),

- SCAO relay optics transmission T_{relay}: 4 relay optics mirrors with protected silver/aluminium coatings (transmission profile from the "ESO database of technical data for E-ELT simulations"),

- SCAO dichroic plate transmission towards MICADO: T_{dichro}=95%,

- SCAO dichroic plate reflection: R_{dichro}=5%,

- MICADO transmission T_{mic}: 5 warm glass optics (one ADC and the entrance window) with individual transmissions of 98%, 5 cold aluminium-coated mirrors (transmission profile from the "ESO database of technical data for E-ELT simulations"), a cold K-band filter (transmission profile from the "ESO database of technical data for E-ELT simulations") and a detector (quantum efficiency of 92%),

- diffusion on the SCAO dichroic plate: ϵ_{dif}=0.5%,

- glass transmission: T_g=98%,

- intrinsic glass transmission: T_{ig}=99.5%,

- pixel scale (primary arm): $pscl$=3 mas/pixel,

- pixel size: 15 microns, hence a pixel area A_{pix}=2.25×10^{-10}m^2,

- telescope focal ratio: 18.85,

- MICADO linear scale: 3838 microns/arcsec.

The f/ratio of warm beam on the detector is then 24.557 (18.85×15/3838/0.003), leading to a corresponding solid angle of 1.302×10^{-3} st (π/4/24.5572) and then to a corresponding pixel area-solid angle product receiving warm radiation: $A_{pix}.\Omega_{pix}$=2.930×10^{-9} cm^2.st.

The sky emission is obtained by multiplying the sky emission outside the atmosphere (from its magnitude) by the atmosphere, telescope, SCAO and MICADO transmissions. The telescope thermal emission is given by integrating over the K-band a Planck law $PL(\lambda,\theta)$ at the ambient temperature θ_{amb}, multiplied by the telescope emissivity ϵ_{tel} (=1-T_{tel}) and the SCAO and MICADO transmissions. The SCAO thermal emission is given by integrating over the K-band a Planck law at the ambient temperature, multiplied by the SCAO emissivity ϵ_{scao} (=1-$T_{relay}.T_{dichro}$) and the MICADO transmission. The MICADO warm optics thermal emission is given by integrating over the K-band a Planck law at the ambient temperature, multiplied by the MICADO warm optics emissivity ϵ_{wmic} (=1-T_{ig}^5) and the MICADO transmission:

$$F_{sky} = \int_{K-band} T_{atm}.T_{tel}.T_{relay}(\lambda).T_{dichro}.T_{mic}(\lambda).10^{-0.4\,m_{sky}}.F_0.A_{tel}.pscl^2.d\lambda \quad (9)$$

$$F_{tel} = \int_{K-band} T_{relay}(\lambda).T_{dichro}.T_{mic}(\lambda).PL(\lambda,\theta_{amb}).A_{pix}.\Omega_{pix}.\epsilon_{tel}.d\lambda \quad (10)$$

$$F_{scao} = \int_{K-band} T_{mic}(\lambda).PL(\lambda,\theta_{amb}).A_{pix}.\Omega_{pix}.\epsilon_{scao}.d\lambda \quad (11)$$

$$F_{mic} = \int_{K-band} T_{mic}(\lambda).PL(\lambda,\theta_{amb}).A_{pix}.\Omega_{pix}.\epsilon_{wmic}.d\lambda \quad (12)$$

MAORY thermal emission top-level requirement states that the AO module thermal emission should not exceed 50% (with a goal of 10%) of the sky+telescope thermal emission. Adopting the same requirement for SAMI, the 50% requirement is met for ambient temperatures up to about 17°C and the 10% requirement is met for ambient temperatures up to about -6°C. Four different options could be considered to decrease the SCAO module background:

- option 1: like in NAOS, implement on the back side of the dichroic plate (the side in front of MICADO) a device - a "background limiter" - that fills up the field of view of MICADO, radiates a very small number of photons and is as black as possible to prevent light scattering.

- option 2: place all the relay optics mirrors and the dichroic plate inside a cooled enclosure.

-option 3: place the dichroic plate inside the MICADO cryostat, assuming the MICADO ADC would be also cooled. In that case, the SCAO thermal emission is limited to the relay optics mirror emission at ambient temperature. The cold optics (inside MICADO cryostat) transmission would then be modified by a factor corresponding to the dichroic plate infrared transmission and the ADC transmission.

- option 4: modify the SCAO module design to use a dichroic plate reflecting the infrared light towards MICADO (instead of transmitting it in the current design) and transmitting the visible light towards the WFS (instead of reflecting it in the current design). From the MAORY study (E. Diolaiti, personal communication), one could expect a dichroic plate infrared reflection of 98%. This dichroic plate being made in BK7, one could expect a visible transmission of 98%.

As a result, the 10% requirement is then reached for ambient temperatures up to 2°C using a background limiter at -30°C, up to 9°C placing SAMI inside a cooled enclosure at -30°C and up to 5°C placing the dichroic plate inside the MICADO cryostat. In practice, the option 1 would require to include this background limiter inside the derotator structure or at the level of the MICADO cryostat itself. A precise mechanical analysis, taking into account the low inclination of the dichroic plate, is required to check for the possibility of such an implementation. The option 2 would require using an enclosure cooled on a rather large surface: the relay optics bench is 2.5m × 3.5 m. Such a large enclosure has been contemplated by MAORY, with an additional mass of 3350 kg. Though an additional difficulty is to include the dichroic plate inside this enclosure, the dichroic plate being located inside the derotator structure. The option 3 would require modifying the MICADO cryostat design. The option 4 would require making a new SCAO design and analysis.

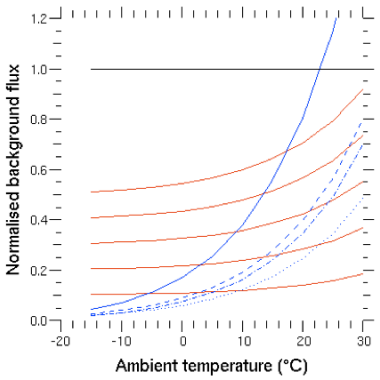

Figure 4. K-band thermal emissions normalized to the sky's one (horizontal line). Slowly increasing curves are 50%, 40%, 30%, 20% and 10% of the sky+telescope thermal emission. Quickly increasing curves are the SCAO thermal emissions for the current design (continuous line) and the options 1 (dashed line), 2 (dotted line) and 3 (dotted-dashed line).

4. ADAPTIVE OPTICS CORRECTION PERFORMANCE

4.1 Atmospheric parameters

The atmospheric parameters adopted for deriving the SAMI performances are extracted from the ESO document *"E-ELT AO design inputs: relevant atmospheric parameters"*. They are summarized in Table 3:

Table 3. Turbulence model parameters

	Turbulence case	Seeing at zenith and 0.5 μm	Zenith angle	Outer scale	v_{mean}	h_{mean}
Value	Median	0.65"	30°	35 m	16.4 m/s	4007 m

Given the 30° zenith angle, the actual seeing is 0.71", corresponding to r_0(0.5 μm)=14.5 cm.

4.2 Error budget decomposition

The global error budget is made of the following contributors:

$$\sigma^2_{tot} = \sigma^2_{fitting} + \sigma^2_{diff\ refr} + \sigma^2_{chrom} + \sigma^2_{alias} + \sigma^2_{temp} + \sigma^2_{noise} + \sigma^2_{DM\ sat} + \sigma^2_{calib} + \sigma^2_{NCPA} + \sigma^2_{aniso} \quad (13)$$

where $\sigma^2_{fitting}$ corresponds to the ability of the deformable mirror to "fit" the turbulence and to the residual cophasing error of the M1 individual mirrors, $\sigma^2_{diff\ refr}$ corresponds to the error resulting in sensing the wavefront at a wavelength different from the imaging wavelength (due to differential refraction the wavefront sensor source does not appear at the same location on sky at these two wavelengths), σ^2_{chrom} corresponds to the error resulting in correcting a wavefront at wavelength different from the imaging wavelength, σ^2_{alias} corresponds to high order aberrations un-measured by the WFS and seen as low order aberrations by the WFS, σ^2_{temp} corresponds to the error made in correcting an aberration measured some time before, σ^2_{noise} corresponds to the classical noise error but includes the effect of windshake, σ^2_{aniso} corresponds, when applicable, to the error made when the reference source and the science target are distant one from the other. $\sigma^2_{DM\ sat} + \sigma^2_{calib} + \sigma^2_{NCPA}$ in our Phase A study, are not specifically analyzed and are assumed equal to 80 nm rms, corresponding to SR=95% in the K-band.

4.3 Fitting error

4.3.1 Turbulence term

We will use the M4 mirror of the E-ELT for correcting the wavefront errors. From the ESO document *Technical specifications for the conceptual design, prototyping, preliminary design of the M4 adaptive unit for the E-ELT*, the fitting error due to turbulence, in nm, is given by: $\sigma_{fitting} = 166 \times seeing^{5/6}$, where *seeing* is given in arcsec. Hence, for a seeing of 0.65" at 30° zenith angle, one derives $\sigma_{fitting}$=125 nm rms. Equalizing this equation with the following one: $\sigma^2_{fitting} = 0.257 J^{-5/6} (D/r_0)^{5/3}$, where $\sigma_{fitting}$ is in radians, one finds the equivalent number J of corrected Zernike modes: 5562.

4.3.2 M1 cophasing error

Little is still know about this error. We assume for this term an error of 50 nm rms.

4.4 Differential refraction error

Due to the differential refraction of the atmosphere with respect to wavelength, resulting from the refraction index dependency with the wavelength, the apparent location on sky of the WFS reference source is different at the WFS wavelength and the imaging wavelength. It can be seen as an anisoplanatism error, with an anisoplanatism angle corresponding the angular distance between the WFS reference source locations at the two wavelengths.

$\theta_{diff\ ref}$ is this angular separation at a zenith angle of 30°, for the reference source at a WFS wavelength of 0.589 μm and an imaging wavelength of 2.2 μm. From the classical differential refraction formulae, one compute $\theta_{diff\ ref}$=0.37" under the typical Paranal atmospheric conditions (http://www.eso.org/gen-fac/pubs/astclim/lasilla/diffrefr.html: T=284.65 K, R_H=14.5% and P=743 mbar). The corresponding error $\theta_{diff\ ref}$ for a 0.71" seeing and L_0=25 m is 10 nm rms, computed using Chassat (1992) (cf. also Section 10.8).

4.5 Chromatism error

From the ATLAS Phase A study (Fusco et al., 2010), for a 0.71" seeing, an outer scale of 25 m, a WFS wavelength of 0.589 μm and an imaging wavelength of 2.2 μm, this error is 25 nm rms.

4.6 Aliasing error

We consider the aliasing error to be 35% of the fitting error.

4.7 Temporal and noise errors

4.7.1 Simulation software

These errors are estimated in two steps, with two home-made simulation tools. The first one is an end-to-end simulation tool of an AO loop for a single Shack-Hartmann subaperture. It allows one to compute the noise error seen by a subaperture, given classical AO simulation parameters. The second tool allows one to compute the noise and temporal errors for the entire Shack-Hartmann given the noise error for a single subaperture, the r_0, L_0 and mean wind speed values, the loop frequency, the number of mirror actuators. This estimation can be made taking into account the windshake residuals by the implementation of a simple Kalman filtering. We describe with more details these two pieces of software in the following.

• *Single aperture simulation*

The goal of this simulation tool is to derive the noise level of the wavefront sensor, in terms of the different parameters of the Hartmann, namely: number of photons per frame, WFS wavelength, seeing, subaperture diameter, sampling frequency, detector readout noise, pixel size, number of pixels, centroiding method (either classical thresholded centre of gravity, or weighted centre of gravity, the latter one being actually used hereafter), loop local gain (equivalent loop gain between the subaperture and M4), wind speed.

Our simulation tool simulates a single SAMI subaperture, on the E-ELT. The behaviour of the deformable mirror M4 is also simulated in front of this subaperture, with a local feedback loop with one frame delay. The program simulates a time-serie of Kolmogorov-like turbulent wavefronts. A high-resolution image of the spot at the focus of the micro-lens is computed, with its centre of gravity. This latter will be used as the reference for computing wave-front sensing errors.

The flux of the high-resolution image is then normalized, and the image resolution is then degraded to the resolution of the Shack-Hartmann wavefront sensor pixels, in order to form the wide pixels of the Hartmann. Some photon noise and read-out noise is added. On this Hartmann image, the centre of gravity is computed using either a given number of different threshold values with thresholded centre of gravity or another given number of different widths of weighting functions.

Finally, the centroiding error is computed for each of the above values, and the minimum error (which allows one to optimize threshold value and width of weighting function) is searched for each simulation.

• *Simulation of an on-axis SCAO system for the E-ELT*

We simulate SAMI as an AO system on Zernike polynomials, up to any arbitrary order (in our case n=84, i.e. J_{max}= 3655 modes). Assuming a Taylor hypothesis, the PSD of a given Zernike mode j is given in the literature by:

$$W_j(\nu) = \int_{-\infty}^{\infty} \|Q_j(\nu/V, y)\|^2 \left((\nu/V)^2 + y^2 + 1/L_0^2 \right)^{-11/6} dy \tag{14}$$

where $Q_j(x, y)$ is the Fourier transform of the mode $Z_j(x, y)$. Having obtained an analytical expression of

$$\sum_{j \in radial\ order} \|Q_j(\nu/V, y)\|^2 \tag{15}$$

we can compute the sum of the PSD of the whole Zernike order, taking the outer scale effects into account.

For each radial order, we compute the real transfer function of an AO loop, with any arbitrary loop delay (for the present study we took 1 frame delay) and integrator gain. We assume that this transfer function is the same for any Zernike mode of the whole radial order, so that we can compute the temporal residual error of the whole order by integrating over frequencies the product between this transfer function by the cumulated PSD of all the Zernike modes of the considered order.

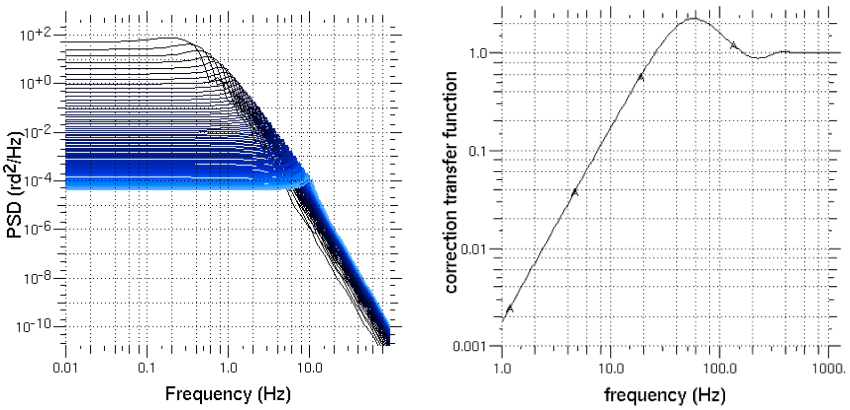

Figure 5. Left: Example of the simulated Zernike spectra, cumulated over the whole radial orders, for D=42 m and L_0=25 m, for n=1 to 84 (the whole computation for the 84 orders takes 5.3 seconds). Right: Example of the simulated loop transfer function for 500Hz sampling frequency and 2ms delay, with an integrator gain of 0.3.

From our single aperture simulation (cf. above) we know, as an input, the noise variance at the sub-aperture level. We propagate spatially this noise onto the Zernike assuming a law in $\sigma_j^2 = 0.3\,\sigma_\phi^2/(n+1)^2$ for each Zernike mode, which leads to the expression of the variance σ_n^2 for the full radial order: $\sigma_n^2 = 0.3\,\sigma_\phi^2/(n+1)^2$.

We then know the level of the noise PSD and are hence able to deduce the noise variance that is propagated into the loop through the transfer function (from an analytical formula). This computation is done for any loop gain from 0 to 0.7 and we select the gain that led to the best performance, i.e. the best compromise between the noise error, increasing with gain, and the temporal error, decreasing with gain: this is a modal optimization.

As a by-product of this process, we can derive the temporal error, the noise error, the optimum system bandwidth for each radial order and the efficiency of the compensation for each radial order.

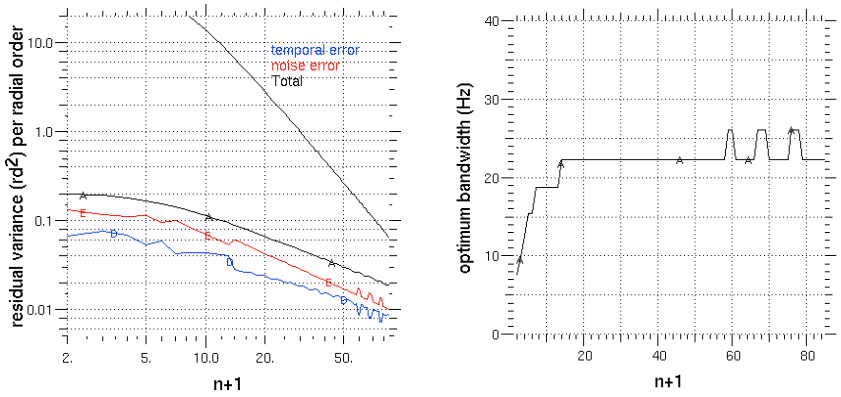

Figure 6. Left: Example of the residual error (temporal and noise ; the upper black curve is uncorrected Zernike variance). Right: Exemple of the optimum bandwidth for r_0=15 cm, D=42, L_0=25 m and 330 nm rms input WFS noise.

Tip-tilt has a special treatment: we add the windshake PSD to the atmospheric PSD. We use an analytical formula that fits the windshake PSD, and we simulate the temporal compensation that could be done by an advanced temporal compensator (such a Kalman filter of an high order). The transfer function of this filter is not modeled very accurately, but with a level of detail suitable for a phase A study only. While a pure integrator would have only a ν^2 law attenuation, the chosen model follows a ν^4 law at low frequency:

$$\|H_{cor}(\nu)\|^2 = \begin{cases} \nu^4/BP^4 & \nu < BP \\ 1 & \nu > BP \end{cases} \tag{16}$$

We compute the propagated noise and perform a modal optimisation with this filter exactly as described above. We treat the radial order n=1 (i.e. tip/tilt) as a whole and do not process tip in a different way than tilt. However, X and Y windshake properties are not the same and we should probably investigate a way to optimize this more finely during a phase B.

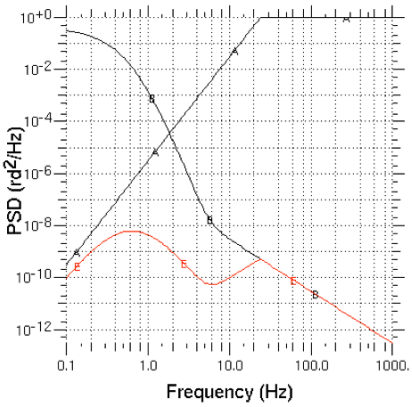

Figure 7. Example of the fitted windshake PSD, the modelled transfer function (with a bandpass of 25 Hz), and the product of both (the lowest curve, in red for colour printing).

4.7.2 Simulation results

Simulations are run assuming:

- V-band zero point: 1×10^{11} photons/s/m^2/μm
- Spectral bandpass: 0.35 microns (0.45-0.8 microns)
- Optical transmission: 0.546 (telescope: 65%, WFS: 84%)
- Detector quantum efficiency: 80%
- No sky background
- WFS wavelength: 0.6 microns
- Zenith angle: 30°
- r_0 at zenith and 0.5 microns: 15.9 cm (i.e. 14.5 cm at 30° zenith angle)
- L_0 at 0.5 microns: 25 m
- Mean wind speed: 16.4 m/s
- Number of subapertures: 84
- Maximum Zernike radial order considered: 84
- Detector readout noise: 3e- rms
- 1 frame delay
- Windshake residual PSD fitted from from ESO data (Fig. 7), corresponding to 0.28 arcsec rms residuals

If the four-quadrant configuration (2×2 pixels/subaperture) almost always gives the lowest noise, other numbers of pixels per subaperture lead to similar values. Given the specific issues of gain calibration of a four-quadrant configuration, one could then favour a 4×4 configuration.

4.8 Anisoplanatism error

This error contribution is estimated using the Chassat (1992) formulae. They allow one to analytically compute the anisoplanatism phase error given a turbulence model. Results, using the atmospheric parameters of Section 4.1 and the ESO atmospheric model, are given in Table 4.

Table 4. Anisoplanatism errors for a seeing of 0.71" and L_0=25 m

Distance from reference source (arcsec)	5	10	15	20	25	30	35	40	45	50	55	60
Anisoplanatism error for L_0=25 m (nm rms)	101	184	253	305	354	396	433	475	518	571	554	579
Corresponding Strehl ratio loss at 2.2 μm	92%	76%	59%	47%	36%	28%	22%	16%	11%	7%	8%	6%

4.9 Global error budget

Table 5. Error budget values in nm rms and corresponding on-axis Strehl ratio at 2.2 microns for different reference star magnitudes

	m_V=12	m_V=13	m_V=14	m_V=15	m_V=16
Turbulence fitting error	125				
M1 cophasing fitting error	50				
Differential refraction error	10				
Chromatism error	25				
Aliasing error	44				
DM saturation, calibration & NCPA error	80				
Temporal and noise error	80	122	181	284	487
Total error	183	205	245	328	514
Corresponding Strehl ratio	76%	71%	61%	41%	12%

5. ADAPTIVE OPTICS CALIBRATIONS

5.1 Reference slope calibrations

The measurement of the reference slopes will be performed thanks to a source positioned at the WFS field stop. The WFS will be moved (in X-Y) in front of this fibre-fed source for this measurement.

A special care will have to be taken to the accurate alignment of this fibre together with the optical axis of the WFS K-mirror. It could be achieved by checking that the beam is not deviated when rotating the K-mirror. An alternative could be to average out the reference slope measurements when rotating the K-mirror.

5.2 Interaction matrix

The measurement of the interaction matrix requires the use (and then the implementation) of a visible point-like source at the E-ELT intermediate focus, between M2 and M3. In addition, this measurement requires delineating physically the pupil. We hence propose to use a pupil mask in front of the micro-lenses.

5.3 Non-common path aberrations

We propose to measure the non-common path aberrations thanks to a classical phase diversity method. It requires using (and then implementing) an infrared point-like source at the E-ELT intermediate focus. An alternative would be to proceed with the phase diversity on sky using a bright source.

5.4 Pupil monitoring

In our design, the pupil shifts are compensated by tilting the M11 mirror. It thus requires monitoring these pupil movements. Different solutions are conceivable for this monitoring:

- measure the illumination of the subpupils at the edge of the Shack-Hartmann. Though, since we contemplate to use a pupil mask in front of the micro-lenses to calibrate the interaction matrix, the pupil shifts would be

inferred only from the lack of illumination of the subpupils at the edge, which is not as robust as inferring these pupil shifts also from the illumination of subpupils oustide the pupil

- infer the pupil shifts from on-sky interaction matrix measurements. This method has been used by E. Gendron during NAOS AIT and is being simulated by H. Bonnet at ESO. Though, we fear that this method could be difficult to apply on faint sources

- measure the pupil shifts using sources at the M4 position, around the mirror, and dedicated (4-quadrants) detector(s) inside the WFS

To our knowledge, none of these methods has been used in operation at telescope. Their feasibility and limitations would have to be studied in a Phase B.

6. CONCLUSION

This study has presented a possible implementation of a SCAO module for MICADO. If few points are still to be confirmed (e.g., the lack of need for an ADC) or investigated (e.g., the pupil movement monitoring), it showed that the MICADO top-level requirements could be fulfilled. First performance estimations, that have to be consolidated in a Phase B, show that such a SCAO module could reach a $\sim$75% Strehl ratio for an on-axis m_V=12 guide star.

References

Chassat, F., PhD thesis, "Propagation optique à travers la turbulence atmosphérique : étude modale de l'anisoplanétisme et application à l'optique adaptative", Université de Paris-Sud, Centre d'Orsay, 1992

Davies, R., et al., "MICADO: the E-ELT Adaptive Optics Imaging Camera," in *Ground-based and Airborne Instrumentation for Astronomy III*, Proc. SPIE, **7735**, 2010

Diolaiti, E., Conan, J.-M., Fioppani, I., et al., "Conceptual design of the multi-conjugate adaptive optics module for the European Extremely Large Telescope," in *Adaptive Optics Systems II*, Proc SPIE, **7736**, 2010

Fusco, T., Meimon, S., Clénet, Y., et al. "ATLAS: the E-ELT laser tomographic adaptive optics system," in *Adaptive Optics Systems II*, Proc SPIE, **7736**, 2010